

Weakly Supervised Intracranial Hemorrhage Segmentation using Head-Wise Gradient-Infused Self-Attention Maps from a Swin Transformer in Categorical Learning

Amirhossein Rasoulian <https://orcid.org/0009-0004-9077-521X> ah.rasoulian@gmail.com
Department of Computer Science and Software Engineering, Concordia University, Montreal, QC, Canada

Soorena Salari <https://orcid.org/0000-0002-2587-0323> soorena.salari374@gmail.com
Department of Computer Science and Software Engineering, Concordia University, Montreal, QC, Canada

Yiming Xiao <https://orcid.org/0000-0002-0962-3525> yiming.xiao@concordia.ca
Department of Computer Science and Software Engineering, Concordia University, Montreal, QC, Canada

Abstract

Intracranial hemorrhage (ICH) is a life-threatening medical emergency caused by various factors. Timely and precise diagnosis of ICH is crucial for administering effective treatment and improving patient survival rates. While deep learning techniques have emerged as the leading approach for medical image analysis and processing, the most commonly employed supervised learning often requires large, high-quality annotated datasets that can be costly to obtain, particularly for pixel/voxel-wise image segmentation. To address this challenge and facilitate ICH treatment decisions, we proposed a novel weakly supervised ICH segmentation method that leverages a hierarchical combination of head-wise gradient-infused self-attention maps obtained from a Swin transformer. The transformer is trained using an ICH classification task with categorical labels. To build and validate the proposed technique, we used two publicly available clinical CT datasets, namely RSNA 2019 Brain CT hemorrhage and PhysioNet. Additionally, we conducted an exploratory study comparing two learning strategies - binary classification and full ICH subtyping - to assess their impact on self-attention and our weakly supervised ICH segmentation framework. The proposed algorithm was compared against the popular U-Net with full supervision, as well as a similar weakly supervised approach using Grad-CAM for ICH segmentation. With a mean Dice score of 0.47, our technique achieved similar ICH segmentation performance as the U-Net and outperformed the Grad-CAM based approach, demonstrating the excellent potential of the proposed framework in challenging medical image segmentation tasks.

Keywords: Weak Supervision, Image Segmentation, Swin Transformer, Intracranial Hemorrhage, Self-attention

1. Introduction

Intracranial Hemorrhage (ICH) is a potentially fatal cerebrovascular disorder that is responsible for 10-15% of all stroke cases and can be caused by various factors, such as head trauma, high blood pressure, and blood clots (Rajashekar and Liang, 2021; Apostolaki-Hansson et al., 2021). The outcome of ICH depends on the volume of bleeding, which can enlarge rapidly within the first few hours (Qureshi and Palesch, 2011), leading to a high risk of secondary brain injury or even death if it is not treated promptly. In general, ICH can be classified into five subtypes based on its location in the brain, including Intraventric-

ular (IVH), Intraparenchymal (IPH), Subarachnoid (SAH), Epidural (EDH), and Subdural (SDH). Note that one patient may have more than one hemorrhage subtype. Each ICH subtype should receive customized treatment approaches, and surgery is only considered if the location of hemorrhage is advantageous. Upon admission at the hospital, early detection and accurate quantification of ICH are critical in selecting appropriate medical interventions and reducing patient mortality. Compared to other medical imaging modalities, such as MRI, computerized tomography (CT) is often used in the clinic to assess ICH due to its fast imaging time and good accessibility.

Recent progresses in deep learning (DL) techniques, especially convolutional neural networks (CNNs), have led to the development of efficient and accurate solutions for computer-assisted diagnosis and treatment decisions. For the care of intracranial hemorrhage, several automatic DL algorithms have been devised for the detection, subtyping, and volumetric segmentation of intracranial hemorrhage based on clinical scans (Hssayeni et al., 2020). While CNNs have provided state-of-the-art performance in various medical imaging applications, their weak ability to encode long-range spatial information due to often limited field of view may affect the accuracy of ICH detection and subtyping, especially considering that the spatial location of hemorrhage is crucial for the learning task and ultimately for diagnosis. To address this shortcoming of CNNs, the Vision Transformer (ViT) (Dosovitskiy et al., 2021) uses multi-head attention mechanisms to encode contextual relationships between spatially distributed image patches and has attracted great interest for vision tasks, including medical imaging applications (Dai et al., 2021; Dalmaz et al., 2022). However, by removing convolutions, the ViT possesses low locality inductive biases, such as translational invariant features. To address this, the Swin transformer (Liu et al., 2021), an efficient hierarchical Transformer was proposed as a recent variant. It gradually reduces the number of tokens by merging image patches and computing attentions in non-overlapping local windows to mitigate the drawback of the ViT. Training CNNs and Transformer-based models requires a significant amount of data, but annotating medical images is a laborious and time-consuming process, particularly for segmentation tasks. Among various strategies, including semi-supervised learning, weakly supervised methods (Zhou, 2017) offer alternative solutions to address such challenges by deriving fine-grained image segmentation from coarse and more accessible image annotations, such as bounding boxes, scribbles, and categorical labels.

In our previous work (Rasoulia et al., 2022), we employed a Swin transformer to perform CT-based detection and weakly supervised segmentation of ICH for the first time. More specifically, we obtained ICH segmentation by fusing hierarchical self-attention maps generated from a Swin transformer that was trained using categorical labels for ICH detection. Furthermore, comparing the proposed weakly supervised ICH segmentation framework for two Swin transformers based on (1) binary classification (presence of hemorrhage or not) and (2) multi-label classification (detailed ICH subtypes and with/without ICH), we found that binary classification helped better focus the network attention on the ICH regions. In this paper, we further extended our previous study (Rasoulia et al., 2022) in three main directions. First, inspired by the gradient-weighted class activation mapping (Grad-CAM) (Selvaraju et al., 2017), we proposed a novel attention visualization technique, called HGI-SAM (Head-wise Gradient-infused Self-Attention Mapping), by performing head-wise weighing of self-attention obtained from the Swin transformer using the gradient of the

target class. We further demonstrated the benefit of incorporating HGI-SAM in our weakly supervised ICH segmentation framework over the original proposal (Rasoulia et al., 2022). Second, by inspecting the characteristics of the gradient-weighted attention maps obtained from ICH detection, we further tailored the post-processing method to optimize the segmentation accuracy. Lastly, with the publicly available RSNA 2019 Brain CT hemorrhage (Flanders et al., 2020) and PhysioNet datasets (Hssayeni et al., 2020), we conducted a comprehensive evaluation of the new method against our previous approaches, a fully supervised U-Net, and a similar weakly supervised segmentation method leveraging the popular Grad-CAM technique, in the tasks of ICH segmentation and detection.

2. Related Works

To overcome the challenge of limited, well-annotated training data in developing deep learning techniques for medical image segmentation, a number of semi-supervised and weakly supervised algorithms have been proposed (Wang et al., 2022; Qureshi et al., 2023). While semi-supervised strategies still leverage a small number of refined image labels through data augmentation, transfer learning, and interactive segmentation to enhance the accuracy and capacity of pre-trained DL models, weakly supervised techniques rely entirely on coarse labels in the formats of bounding boxes (Rajchl et al., 2017), scribbles (Liu et al., 2022), points (Roth et al., 2021), or even categorical labels (Lin et al., 2018). As these coarse-level labels are more economical to acquire, weakly supervised segmentation techniques can further reduce the need for refined pixel/voxel-level annotations. With simple bounding boxes, Rajchl et al. (2017) proposed DeepCut, an approach that combined a CNN segmentation model with a densely-connected conditional random field (CRF) in an iterative training process to achieve pixel-level segmentation. Their method was tested on brain and lung segmentation for fetal MRI datasets. Following the approach, Kervadec et al. (2020) employed global constraints derived from box annotations, including tightness prior and global background emptiness, to achieve improved segmentation results over DeepCut (Rajchl et al., 2017) on the PROMISE12 dataset (Litjens et al., 2014). Previously, scribble and point annotations have been widely used in interactive segmentation. In weakly supervised segmentation, Roth et al. (2021) employed the random walker algorithm to generate coarse image-level labels from anatomical landmarks, which were used in combination with the point clouds to refine the segmentation results. More recently, Liu et al. (2022) proposed a weakly supervised COVID-19 infection segmentation method based on image scribbles and an uncertainty-aware mean teacher framework. To further alleviate the need for pixel/voxel-wise manual annotation, weakly supervised segmentation methods that solely rely on categorical labels are highly attractive. With the assumption that deep neural networks in image classification tasks should have local focus on the target objects, this type of approach was made possible by the latest techniques that provide an intuitive visual explanation of the reasoning process for DL algorithms through saliency, class activation, and attention maps. In this domain, Han et al. (2022) proposed a weakly supervised segmentation model based on class residual attention for the lung adenocarcinoma and breast cancer datasets. Chen et al. (2022) developed a novel class activation mapping for weakly supervised segmentation for MRI datasets that achieves a state-of-the-art accuracy, and similarly, Viniavskyi et al. (2020) utilized class activation maps for Chest X-Ray segmentation. With the transformer

model, Li et al. (2023) utilized a self-attention mechanism in multiple instances learning for weakly supervised segmentation of histopathology images.

Almost all previous reports on automatic ICH detection and/or segmentation primarily relied on supervised learning strategies. Hssayeni et al. (2020) recently conducted a comprehensive review of these techniques in both semi-automatic and automatic manners, and binary classification (ICH versus non-ICH) achieved an area-under-the-curve (AUC) of 0.846~0.975, while more fine-grained ICH subtyping achieved an AUC of 0.93~0.96. Deep learning-based approaches in ICH detection typically used fully convolutional networks (FCNs) (Cho et al., 2018) and recurrent neural networks (RNNs) (Ye et al., 2019), and their accuracy was generally higher for ICH versus non-ICH classification than for ICH subtyping. Following the trend in explainable artificial intelligence (XAI), attention mechanisms have been employed to both boost the detection accuracy and visually illustrate classification results (Salehinejad et al., 2021). Furthermore, very limited attempts were also made to apply the attention/class activation in weakly supervised brain lesion and hemorrhage segmentation (Wu et al., 2019; Nemcek et al., 2021). Specifically, Wu et al. (2019) used refined 3D Class-Activation Maps (CAMs) to segment stroke lesions from the Ischemic Stroke Lesion Segmentation (ISLES) dataset (multi-spectral MRI), and achieved a 0.3827 mean Dice score. Likewise, Nemcek et al. (2021) found the location of ICH as bounding boxes in axial brain CT slices based on the regional extrema of attention maps acquired from a ResNet-like binary classification CNN. In their approach, a mean Dice of 0.58 was reached for the lesion bounding boxes. Unfortunately, to the best of our knowledge, aside from our earlier work (Rasoulilian et al., 2022), self-attention, especially with a Swin transformer, has not yet been explored for weakly supervised ICH segmentation, and we intend to further improve our proposed framework to boost the performance.

3. Methods

An overview of our proposed weakly supervised technique for ICH segmentation is depicted in Fig. 1, which comprises two major components. First, a Swin transformer was trained through an ICH detection task using categorical labels (ICH vs. without ICH). Then, during test time, the segmentation module utilized hierarchical attention maps from the Swin transformer blocks along with their corresponding gradients to predict the hemorrhage segmentation map. Due to high variability in slice thicknesses among the CT data, we decided to implement our algorithm based on 2D axial slices. The details of the methodology are provided in the following sections.

3.1 ICH detection with a Swin transformer

In our proposed technique, we employed the Swin-Base transformer architecture, which divides an input image into 4×4 patches before passing their embedding through 4 layers/hierarchies to predict the existence of hemorrhages. Unlike the ViT, which computes the multi-head self-attention (MSA) between all image patches, in Swin-Base transformer, self-attention is derived within non-overlapping windows of 12×12 patches, which considerably reduces the computational cost. Here, for simplicity, we will refer to the Swin-Base transformer as “Swin transformer” from this point on. Two main mechanisms help establish the associations between patches across different windows. First, the Patch-Merging

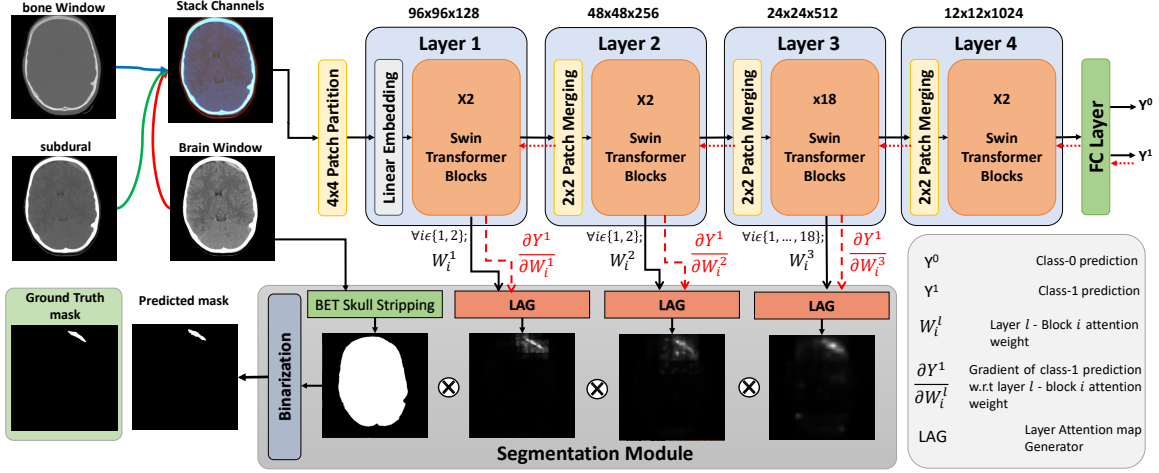


Figure 1: Overview of the proposed weakly supervised segmentation method using hierarchical fusion of gradient-weighted self-attention maps.

module at the beginning of each Swin transformer layer combines and encodes every 2×2 neighboring patches into one. Second, every two consecutive transformer blocks apply window-based multi-head self-attention (W-MSA) and shifted window-based multi-head self-attention (SW-MSA) units to input tokens (see Fig. 2a). The self-attention within each window is computed as:

$$\begin{aligned} \text{Attention}(Q, K, V) &= A(Q, K)V, \\ A(Q, K) &= \text{Softmax}\left(\frac{QK^T}{\sqrt{d}} + B\right) \end{aligned} \quad (1)$$

where Q , K , and V denote query, key, and value matrices, respectively. $A(Q, V)$ is the attention weight that we use to derive the attention map, d is the dimension of the query or key, and B is the positional embedding matrix.

In our earlier study (Rasoulia et al., 2022), we discovered that providing additional information (hemorrhage subtypes) to “ICH vs. without ICH” classification during training can distract the network attention in the Swin transformer. As a result, for our new method with HGI-SAM, we decided to establish the backbone of our algorithm based on simple binary ICH detection. To benefit from the target class gradient, instead of using one output neuron to represent the classification outcome, we framed the final network with a two-class setup (i.e., positive and negative ICH detection). Further information of network training is detailed in Section 4.3.

3.2 Hemorrhage Segmentation

In our previous study (Rasoulia et al., 2022), we have qualitatively demonstrated the superior performance of self-attention maps than the class-activation maps obtained with Grad-CAM in visually explaining the ICH detection process in Swin transformers. Therefore, we continued to take advantage of self-attention maps, with a novel formulation to

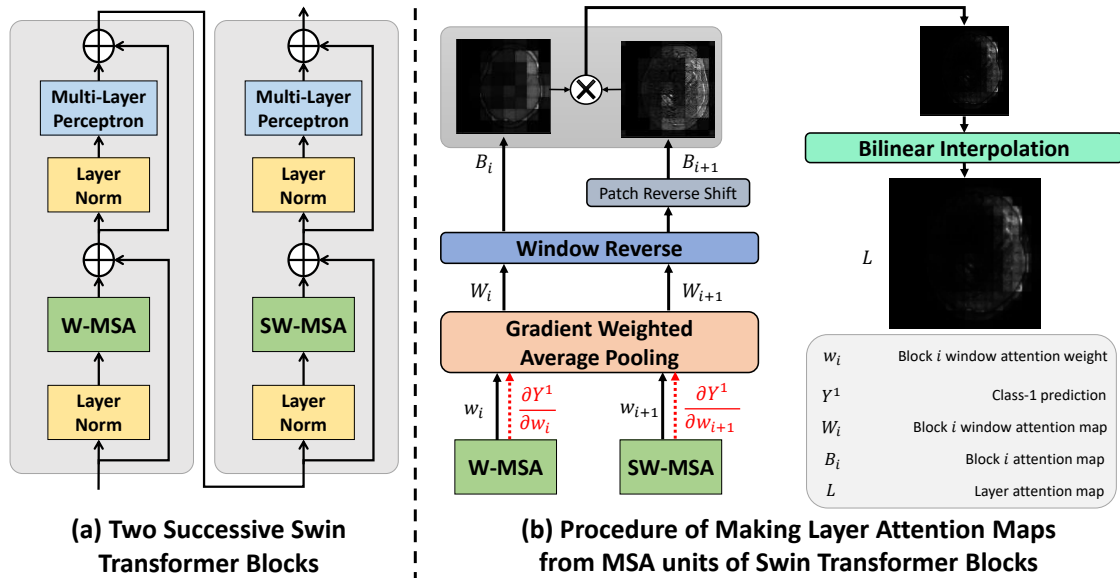


Figure 2: Demonstration of head-wise gradient-infused layer attention map generation in the proposed Swin transformer in categorical learning

perform weakly supervised ICH segmentation. Previous attempts to visualize attention weights in the ViT involved inserting an extra classification token into the image patches and then extracting the attention weight of this token after multiplying the weights of all layers (Chefer et al., 2021; Dosovitskiy et al., 2021). However, this approach is not feasible for the Swin transformer due to its window division mechanisms for both regular and shifted windows. Additionally, multiplying different attention weights is challenging due to two reasons. First, at different layer/hierarchy, Patch-Merging results in different feature map resolution and number of tokens. Second, every two successive Swin transformer blocks have attention weights corresponding to regular and shifted image patches that do not match. To address these challenges, we calculated the attention map at each layer by averaging over all query tokens with additional operations of window and shift reversal, and then the interpolated maps at different layers are multiplied.

3.2.1 LAYER ATTENTION MAP GENERATION

There has been recent research that leverages model classification scores for attention explainability. For instance, Chefer et al. (2021) utilize the Taylor Decomposition principle to assign and propagate a local relevance score through the layers of a ViT model. Similarly, Sun et al. (2021) and Barkan et al. (2021) employ attention gradient weighting on ViT and BERT models, respectively. However, these approaches primarily focused on the attention weight of the “cls” token, and the latter two methods weighed each token’s attention weight through element-wise multiplication. In contrast, our work places emphasis on weighing different heads in multi-head self-attention, and we performed the operation on the more complex Swin Transformer for the first time.

The use of multiple heads in the self-attention mechanism enhances the representational capacity and robustness of the transformer model, as each head can focus on different aspects of the input and learn a unique set of attention weights, thus capturing more complex relationships among the tokens. However, this critical fact was overlooked in most previous attention map generation methods (Gao et al., 2021), including our own previous work (Rasoulia et al., 2022). In the existing literature, a naive averaging is often applied to the attention weights of all heads to obtain an overall weight representation. However, as proved by Voita et al. (2019), some heads have more contribution in the output prediction. In this work, we weighed each head by the norm of its gradient regarding the classification score of positive ICH detection, which caused the attention weights of the heads that are more strongly associated with hemorrhage detection to have heavier influence on the final attention weight representation. This is similar to Grad-CAM, where target class gradient is used to weigh the associated activation map to enhance its specificity. As illustrated in Fig. 2, the attention map is created for every two successive blocks as follows:

$$W_i = \frac{\sum_{h=1}^H w_{ih} \times \left\| \frac{\partial Y^1}{\partial w_{ih}} \right\|}{H}, \quad (2)$$

$$L = \text{BI}(\text{WR}(W_i) \times \text{RS}(\text{WR}(W_{i+1})))$$

where w_i is the MSA weight of block i , H is the number of heads in the multi-head self-attention unit, and L is the layer attention map. BI refers to bilinear interpolation, which is utilized to upsample the map to the image size. WR stands for Window Reverse operation, which involves concatenating maps of all windows to create a full image map. Also, RS denotes the reverse shift operation, which is used to reposition the shifted patches of the SW-MSA unit to their original locations in the image. It is good to mention that for Layer 3 in our Swin transformer, which consists of 18 blocks, the final layer map is obtained by averaging the results of 9 maps computed as above.

3.2.2 SEGMENTATION MODULE

The attention map generated by the last layer in the Swin transformer tends to be much more coarse due to the interpolation of a 12×12 pixel map to the image size, resulting in reduced resolution and potential loss of fine-grained details. Therefore, unlike our previous approach (Rasoulia et al., 2022), which used the attention of Layer 4 to compensate for its limited ability to capture relevant features in earlier layers, with the new technique using HGI-SAM, we used the attention maps from the first 3 layers to generate the final ICH segmentation (Zhou et al., 2021). Furthermore, as demonstrated in Fig. 1, we employed an additional post-processing step in our approach. This involved multiplying the final fused attention map with a brain binary mask, removing any irrelevant attention weights to ICH segmentation outside the brain region. The skull-stripping procedure was conducted following the recommended steps outlined by Muschelli (2019). Lastly, the refined attention map was binarized using a simple thresholding method, which was demonstrated to be more robust than K-means or Otsu’s method in our previous study (Rasoulia et al., 2022), resulting in a discrete segmentation mask. To determine the optimal threshold value, we conducted a grid search using the validation data.

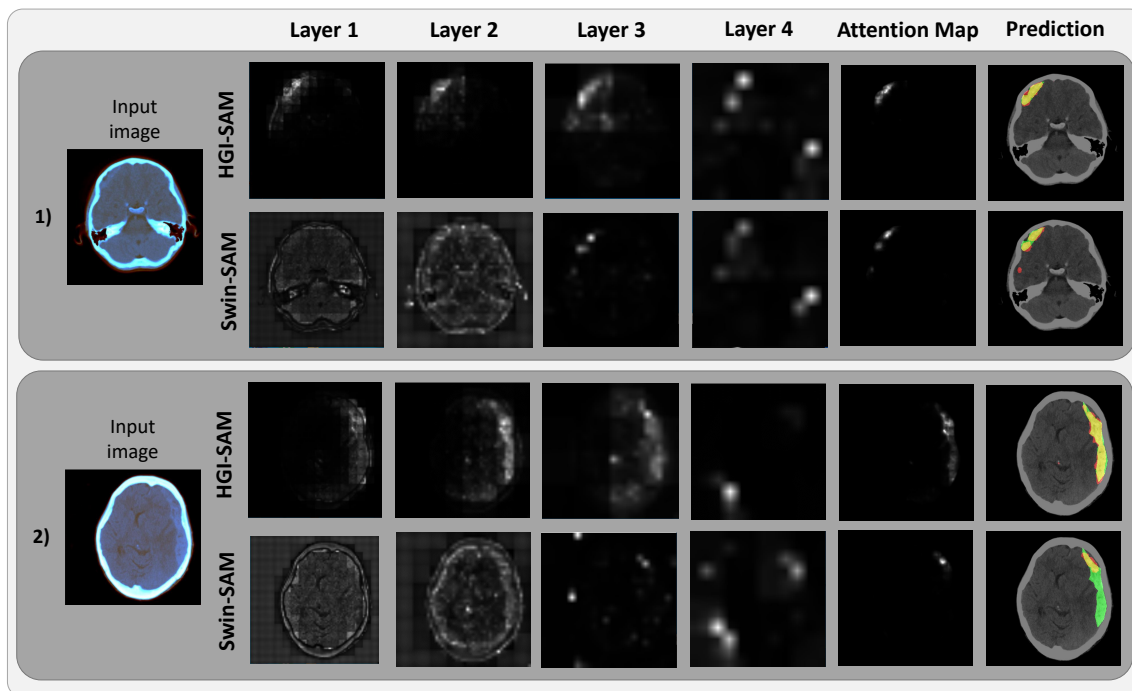


Figure 3: A comparison of the proposed head-wise gradient-infused self-attention mapping (HGI-SAM) and the original self-attention maps (Swin-SAM) from the Swin transformer model is shown for two axial CT slices. Along with the maps at different hierarchies, the fused attention maps and the derived binary ICH segmentation (in red) are also shown over the ground truths (in green).

4. Experiments and Evaluation

4.1 Experimental Setup

To investigate the performance of the proposed weakly-supervised ICH segmentation method using our new HGI-SAM technique, in addition to the approaches from our previous publication (Rasoulilian et al., 2022), we also implemented two baseline models, including a fully supervised U-Net and a similar weakly supervised segmentation method based on binary ICH detection using class activation maps from Grad-CAM. To facilitate the discussion of these methods, we refer the weakly supervised segmentation techniques with Grad-CAM, self-attention maps in multi-label learning (ICH subtyping), self-attention maps in binary ICH detection, and head-wise gradient-infused self-attention maps in binary ICH detection as Swin-Grad-CAM, Swin-SAM Multi-label, Swin-SAM Binary, and Swin-HGI-SAM, respectively. For all Swin-based methods, the DL models were trained using the RSNA ICH CT dataset (Flanders et al., 2020), which contains 752,803 CT slices, with each slice annotated with ICH subtypes, and tested with the PhysioNet CT dataset (Hssayeni et al., 2020) that has 2,814 CT slices with both manual ICH segmentation and ICH subtypes. For each CT slice, brain, subdural and bone windows created using the suggested parameters

provided in the relevant data publications (Hssayeni et al., 2020; Flanders et al., 2020) were stacked to create a three-channel image, downsampled to 384×384 pixels, and normalized using min-max scaling to the range of $[0,1]$. Here, The training dataset (RSNA2019 ICH) was randomly split into 90% and 10% for the training and validation sets. For the fully-supervised U-Net, a five-fold cross-validation was used to build and test the model using only the PhysioNet CT data. Finally, all our networks were trained on a desktop computer with an Intel Core i9 CPU and an NVIDIA GeForce RTX 3090 GPU with 24 GB of memory. The model training details of different segmentation techniques and the evaluation metrics are provided in the following sections.

4.2 ICH segmentation with Swin-SAM Multi-label and Swin-SAM Binary

In our previous work (Rasoulia et al., 2022), two Swin transformers (Wightman, 2019) were trained with categorical learning to provide self-attention maps for ICH segmentation, with one for binary ICH detection and the other for binary ICH detection and full subtyping. When training both models, we used the AdamW optimizer with an initial learning rate of $1e-5$ and early stopping with patience of 3 to avoid overfitting. To address the class imbalance (ICH vs. without ICH) issue in the dataset, we used the focal cross-entropy loss function. Finally, we employed data augmentation techniques, including random left-right flipping, image rotation, and Gaussian noise addition, to improve the capacity and robustness of the trained models. At test time using the PhysioNet data, the binary hemorrhage segmentation was obtained using the same post-processing step as described in Section 3.2.2. More specifically, a five-fold cross-validation approach was used to determining the optimal threshold to generate binary ICH segmentation masks from the fused attention maps. Additionally, the division of the five folds was made consistent with the training and testing of the supervised U-Net model.

4.3 ICH segmentation with HGI-SAM

The Swin transformer for our new weakly supervised ICH segmentation using HGI-SAM was established based on that of the Swin-SAM Binary technique, following our previous insight regarding the benefit of binary classification on self-attention maps (Rasoulia et al., 2022). To allow the computation of class-specific gradients for HGI-SAM, instead of one neuron to represent binary ICH detection outcomes, the new model was equipped with two output neurons to represent the ICH positive class and ICH negative class. To take advantage of our existing work, the new model was fine-tuned based on the Swin transformer backbone of Swin-SAM Binary, using the AdadmW optimizer with a learning rate of $1e-6$ and early stopping. Here, data augmentation with random spatial transformations and Gaussian noise addition was used during training. Furthermore, with the cross-entropy loss function, during training we adopted data sampling that drew training data samples with probabilities that were inversely proportional to their label frequencies to handle the class imbalance issue in the datasets. Upon completing the training, pixel-wise ICH masks were obtained in the same manner as described in the previous section to allow consistent comparison for all techniques.

4.4 Fully supervised U-Net

The U-Net is one of the most popular DL models in medical imaging applications. Therefore, we implemented a fully supervised U-Net model with a lighter architecture than that in the PhysioNet ICH data paper (Hssayeni et al., 2020), which has four hierarchies in the encoding and decoding paths, but less embedding dimension. We used the AdamW optimizer with an initial learning rate of 1e-3, the same sampling and augmentation strategy as our weakly supervised models, and a loss function made of Dice coefficient and cross-entropy, in a five-fold cross-validation setup.

4.5 ICH segmentation with Grad-CAM

As most existing weakly supervised segmentation techniques relied on Grad-CAM, we also implemented another baseline technique, where we employed the class activation map obtained from the final block of the same Swin transformer that we trained with the binary ICH detection task for Swin-HGI-SAM. Similar to the proposed self-attention-based method, the activation map was first multiplied by the brain mask and then thresholded to achieve the final hemorrhage segmentation as described in Section 4.2.

4.6 Evaluation metrics

For all the proposed and implemented methods, we evaluated their segmentation performance using Dice coefficient and Intersection over Union (IoU). In addition, to assess the performance of binary ICH detection, we also computed a range of metrics, including accuracy, area under the curve (AUC), precision, F1-score, recall, and specificity for all algorithms. Note that for Swin-SAM Multi-label, where the designated Swin transformer was trained for both binary ICH classification and subtyping, the performance was assessed only based on the binary detection results. For the U-Net model, ICH detection was recorded as whether the network provided a hemorrhage segmentation for a given image since a similar approach was also used for assessing aneurysm detection in the ADAM MICCAI Challenge (Timmins et al., 2021). It is worth mentioning that to make the performance of U-Net in ICH detection more robust, we do not consider tiny foregrounds as positive ICH (< 10 pixels). As the data division for five-fold cross-validations for different techniques was the same, we reported the ICH segmentation and detection accuracy for all folds. Lastly, two-sided paired sample t-tests were performed to further confirm the performance of our newly proposed segmentation method based on HGI-SAM against the rest of the comparing group.

5. Results

To demonstrate the impact of gradient-weighting for self-attention maps and thus the final hemorrhage segmentation, we illustrate the layer-wise attention maps, along with the combined map and the binary segmentation in Fig. 3 for the axial CT slices of two patients. From Fig. 3, it is evident that the proposed head-wise gradient-infused self-attention maps (HGI-SAM) provided more attention weights with higher specificity for the hemorrhage regions, especially at the first two layers with higher resolutions. This, in turn, provided final binary segmentations with a better agreement with the ground truths. To showcase

the segmentation performance of the proposed method, the results of all mentioned techniques are shown for four different patients in Fig. 4. When comparing Swin-Grad-CAM and the self-attention-based results, we can see that while Swin-Grad-CAM could focus on the general region-of-interest correctly, it often provided much larger segmentations than needed. Between Swin-SAM Multi-label and Swin-SAM Binary, as we discovered in the previous study (Rasoulilian et al., 2022), binary classification helped better focus the model attention in the hemorrhage region than the multi-label counterparts, thus offering more accurate segmentation. Finally, in contrast to the rest of the weakly supervised methods, Swin-HGI-SAM gave the most similar results to the fully supervised U-Net, and notably, in Case 2, the U-Net missed the small ICH that Swin-HGI-SAM was able to identify.

Following the qualitative demonstration of the segmentation performance, the Dice coefficient and IoU metric for all methods are listed in Table 1 for all five folds from the experiments, with their subject-wise mean \pm std. While the U-Net achieved a Dice of 0.506 ± 0.340 and an IoU of 0.406 ± 0.302 in a fully supervised setting, Swin-HGI-SAM was able to offer the second best results, with a 0.465 ± 0.257 Dice and a 0.338 ± 0.214 IoU. With Swin-Grad-CAM as the worst method, Swin-SAM multi-label and Swin-SAM binary performed worse than the newly proposed technique. In terms of statistical tests for segmentation metrics, Swin-HGI-SAM outperformed all weakly supervised methods ($p < 0.05$) while producing similar segmentation accuracy as the fully supervised U-Net ($p > 0.05$).

Finally, in Table 2, we listed the full assessment of ICH detection for Swin-SAM multi-label, Swin-SAM binary, Swin-HGI-SAM, and U-Net. Although U-Net was capable of providing superior ICH segmentation results, its ICH detection accuracy is not satisfactory against the Swin transformer models that were trained with categorical labels. For all Swin transformer models, they offered similar ICH detection performance across all evaluation metrics. By comparing Table 1 and Table 2 across different data folds, we noticed that the detection results align with segmentation performance, especially for weakly supervised based models. This is expected due to the nature of the proposed weakly supervised segmentation framework.

6. Discussion

In recent years, the urgent need to enhance the transparency of deep learning algorithms has encouraged the development of various techniques to visualize network activation/attention maps in vision tasks. Among them, Grad-CAM (Selvaraju et al., 2017) has gained popularity to reveal the regions of interest in image classification tasks for CNNs, thanks to its simplicity and flexibility. Furthermore, extending its original purpose, it has also been adopted in weakly supervised image segmentation based on categorical and metric learning to generate pixel-level semantic labels (Chen et al., 2022), including applications for stroke lesion segmentation (Wu et al., 2019; Nemcek et al., 2021). Compared with Grad-CAM and its variants, the more recent attention mechanisms, especially self-attention from Transformer models, can identify more discriminative, task-related regions and features while improving the performance of the DL models (Liang et al., 2022; Dosovitskiy et al., 2021). This was confirmed in this study when comparing the segmentation performance of the proposed weakly supervised ICH segmentation approaches with Grad-CAM and self-attention maps. As for the self-attention mechanism, different learning strategies may influence the

Table 1: Assessment of ICH segmentation performance for Swin-Grad-CAM, Swin-SAM Multi-label, Swin-SAM binary, Swin-HGI-SAM, and UNet algorithms, using Dice coefficient and Intersection over Union (IoU). All results are reported as mean \pm std.

Fold	Dice Coefficient				
	Swin-Grad-CAM	Swin-SAM Multi-label	Swin-SAM Binary	Swin-HGI-SAM	Fully supervised UNet
1	0.260 \pm 0.180	0.279 \pm 0.167	0.429 \pm 0.185	0.509 \pm 0.245	0.494 \pm 0.322
2	0.176 \pm 0.199	0.201 \pm 0.211	0.341 \pm 0.233	0.357 \pm 0.278	0.404 \pm 0.360
3	0.298 \pm 0.214	0.380 \pm 0.238	0.477 \pm 0.255	0.495 \pm 0.259	0.526 \pm 0.393
4	0.220 \pm 0.227	0.335 \pm 0.255	0.355 \pm 0.225	0.442 \pm 0.277	0.495 \pm 0.328
5	0.276 \pm 0.208	0.353 \pm 0.189	0.425 \pm 0.146	0.525 \pm 0.184	0.613 \pm 0.254
mean \pm std	0.211 \pm 0.245	0.309 \pm 0.223	0.405 \pm 0.218	0.465 \pm 0.257	0.506 \pm 0.340

Fold	Intersection over Union				
	Swin-Grad-CAM	Swin-SAM Multi-label	Swin-SAM Binary	Swin-HGI-SAM	Fully supervised UNet
1	0.162 \pm 0.124	0.173 \pm 0.117	0.290 \pm 0.147	0.373 \pm 0.198	0.387 \pm 0.282
2	0.111 \pm 0.136	0.128 \pm 0.143	0.230 \pm 0.181	0.254 \pm 0.218	0.321 \pm 0.312
3	0.195 \pm 0.159	0.260 \pm 0.180	0.347 \pm 0.208	0.365 \pm 0.220	0.451 \pm 0.359
4	0.144 \pm 0.162	0.231 \pm 0.197	0.238 \pm 0.171	0.324 \pm 0.232	0.391 \pm 0.293
5	0.178 \pm 0.151	0.231 \pm 0.153	0.281 \pm 0.122	0.377 \pm 0.176	0.483 \pm 0.232
mean \pm std	0.150 \pm 0.158	0.205 \pm 0.167	0.277 \pm 0.173	0.338 \pm 0.214	0.406 \pm 0.302

Table 2: Assessment of ICH detection performance for Swin-SAM Multi-label, Swin-SAM binary, Swin-HGI-SAM, and UNet algorithms, using accuracy, AUC, precision, F1-score, recall, and specificity. Note that the mean and standard deviations are computed based on 5-fold cross-validation.

Fold	Accuracy				AUC			
	Swin-SAM Multi-label	Swin-SAM Binary	Swin-HGI-SAM	UNet	Swin-SAM Multi-label	Swin-SAM Binary	Swin-HGI-SAM	UNet
1	0.954	0.961	0.949	0.613	0.898	0.964	0.971	0.782
2	0.918	0.908	0.877	0.489	0.797	0.784	0.788	0.664
3	0.952	0.956	0.952	0.709	0.844	0.873	0.878	0.768
4	0.959	0.959	0.945	0.663	0.827	0.834	0.871	0.755
5	0.982	0.980	0.980	0.561	0.928	0.940	0.947	0.746
mean \pm std	0.953 \pm 0.023	0.953 \pm 0.027	0.941 \pm 0.038	0.607 \pm 0.086	0.859 \pm 0.053	0.879 \pm 0.074	0.891 \pm 0.072	0.743 \pm 0.046

Fold	Precision				F1-score			
	Swin-SAM Multi-label	Swin-SAM Binary	Swin-HGI-SAM	UNet	Swin-SAM Multi-label	Swin-SAM Binary	Swin-HGI-SAM	UNet
1	0.776	0.753	0.685	0.224	0.800	0.847	0.813	0.366
2	0.641	0.588	0.473	0.169	0.641	0.606	0.555	0.284
3	0.849	0.831	0.794	0.260	0.769	0.797	0.787	0.397
4	0.977	0.956	0.923	0.235	0.785	0.789	0.828	0.371
5	0.982	0.933	0.919	0.201	0.915	0.911	0.912	0.334
mean \pm std	0.845 \pm 0.144	0.812 \pm 0.149	0.759 \pm 0.188	0.218 \pm 0.035	0.782 \pm 0.098	0.79 \pm 0.114	0.779 \pm 0.134	0.35 \pm 0.044

Fold	Recall (Sensitivity)				Specificity			
	Swin-SAM Multi-label	Swin-SAM Binary	Swin-HGI-SAM	UNet	Swin-SAM Multi-label	Swin-SAM Binary	Swin-HGI-SAM	UNet
1	0.825	0.968	1.000	1.000	0.970	0.960	0.942	0.564
2	0.641	0.625	0.672	0.891	0.954	0.944	0.904	0.437
3	0.703	0.766	0.781	0.844	0.984	0.980	0.974	0.691
4	0.656	0.672	0.750	0.875	0.998	0.996	0.992	0.635
5	0.857	0.889	0.905	0.984	0.998	0.912	0.990	0.507
mean \pm std	0.737 \pm 0.099	0.784 \pm 0.144	0.822 \pm 0.13	0.919 \pm 0.069	0.981 \pm 0.019	0.958 \pm 0.033	0.96 \pm 0.037	0.567 \pm 0.101

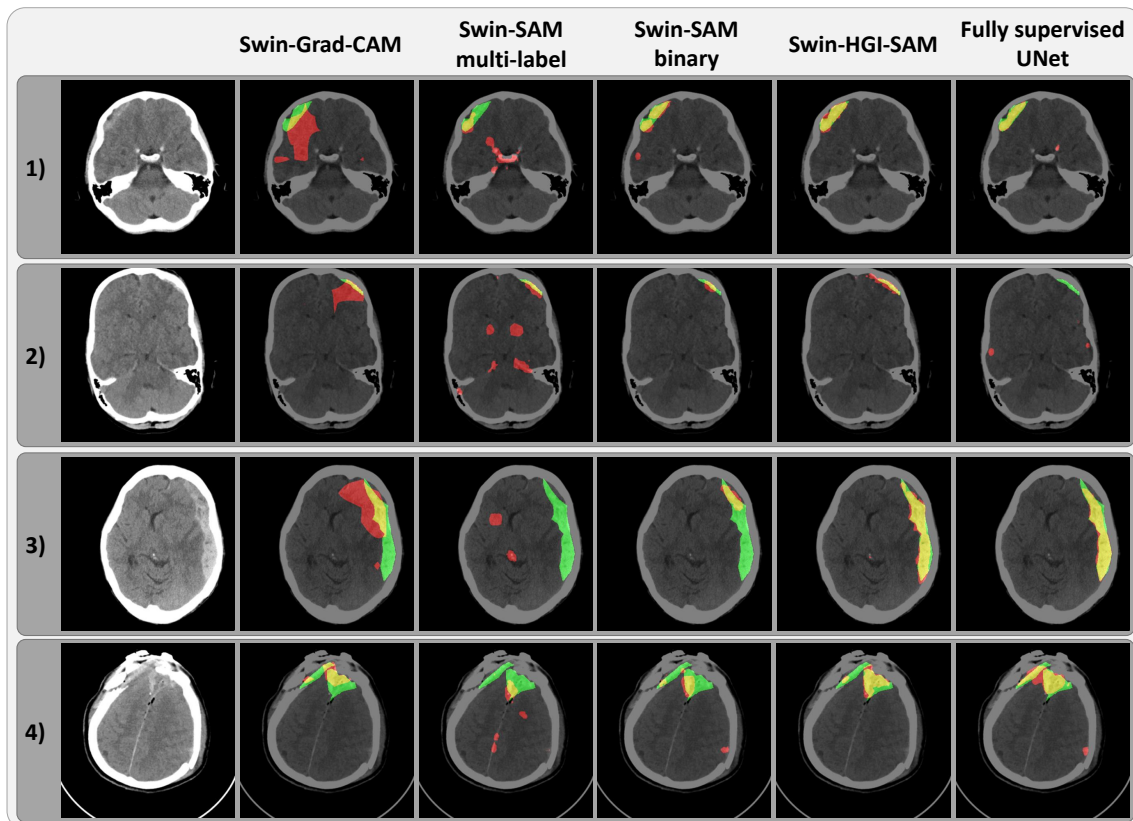


Figure 4: Qualitative comparison of segmentation performance for the proposed weakly supervised ICH segmentation methods (Swin-Grad-CAM, Swin-SAM Multi-label, Swin-SAM binary, and Swin-HGI-SAM) and the fully supervised U-Net for four different cases. Here, red=automatic segmentation and green=ground truths.

positioning and tightness of network attentions with respect to the target objects, and thus the downstream segmentation outcomes in the proposed framework. As an ablation study of our previous work (Rasoulia et al., 2022), we examined the impact of binary (presence of hemorrhage or not) versus multi-label classifications (ICH subtypes and with/without ICH) on self-attention maps from Swin transformers. Using segmentation accuracy as a metric, we found that binary classification helped the network better focus on the hemorrhage regions while both strategies offer similar performance for ICH detection. In the new segmentation method with HGI-SAM, we followed our earlier insights to build our algorithm.

Inspired by the popular Grad-CAM technique (Selvaraju et al., 2017), we incorporated head-wise gradient-weighting for self-attention maps to boost the presentation of the weights relevant to specific class activation for the first time. Compared with other attention mapping technique (Chefer et al., 2021; Sun et al., 2021) that relied on the ViT, we were also the first to implement it on the more complex Swin transformer that was intended to improve

upon the ViT. The enhanced visualization of the attention maps and ICH segmentation accuracy are evident in Fig. 3 and Fig. 4, respectively. Among the obtained attention-maps at different hierarchies, those from the earlier layers contained the relevant attention weights at higher resolutions, and thus were more helpful to delineate the regions-of-interests (i.e., hemorrhages) through the ICH classification task. In our experiment, the head-wise gradient-infused attention map (HGI-SAM) from Layer 4 poses relatively less discriminative power primarily due to much lower resolution and the adverse cascading effect of transformer architecture (Zhou et al., 2021). Therefore, we chose to fuse those from the first three layers for our proposed method. In fact, with a few cases, we found that the fused attention map from the first 3 layers offered better segmentation accuracy than using those from all 4 layers. In our original study that relied on self-attention maps alone, fusing all 4 layers was more beneficial. To obtain discrete ICH segmentation from the HGI-SAM, we applied additional post-processing steps. One major procedure that was different from our original article was multiplying the brain mask before ICH mask binarization. When closely inspecting the attention maps from ICH classification, we noticed that skull fractures were also identified in addition to the hemorrhage. This is likely because for many ICH patients, the condition may result in accidental falls that cause additional injury, such as skull or spine fractures. This phenomenon perfectly showcased the power of attention visualization in explaining the decision-making process in DL models. By constraining the post-processing in the brain region, we intended to exclude the attention weights regarding skull fractures, and were able to further improve the segmentation accuracy. Finally, different from our previous approach (Rasoulia et al., 2022), where the denoised brain window was multiplied to the attention map, our new method directly performed thresholding on the gradient-weighted map to avoid potential intensity inconsistency within the hemorrhage and multi-center imaging protocols. This also allowed us to directly probe the quality of activation/attention maps with respect to their specificity in focusing on ICH.

To provide a baseline for our weakly supervised segmentation framework, we have trained a fully supervised U-Net with the PhysioNet data to perform ICH segmentation. By using data sampling to tackle class imbalance in training, our U-Net model has achieved an improved mean Dice score of 0.506 over that of 0.315 reported for the U-Net in the original data paper (Hssayeni et al., 2020). In comparison, our proposed method has achieved similar results to our supervised U-Net ($p > 0.05$), showcasing the feasibility and excellent potential of weakly supervised segmentation with much more accessible categorical labels. In terms of computational cost, U-Net was the most efficient model, taking only around 10ms/sample, likely due to its simple convolutional layer architecture. On the other hand, Swin-SAM models took around 30ms/sample, and Swin-HGI-SAM and Swin-Grad-CAM took approximately 60ms and 90ms per sample, respectively. This is because the latter two required backward operations for gradient computation. Despite these slightly longer inference times, all these models are still relatively fast and suitable for clinical setups, offering practical benefits.

While there is still room for improvement in our future work, ICH segmentation from clinical scans remains a challenging task at the moment. In our proposed framework, extracting meaningful pixel-wise attention maps is crucial. We are aware that the exploration on self-attention in this study may be data-, application- and model-specific. We will continue to investigate the characteristics of self-attention in different learning strategies,

extended applications, and other Transformer models in the future. These would be greatly beneficial to improve weakly supervised medical image segmentation based on categorical labels. Incorporating inter-slice or 3D spatial information may be beneficial to the designated tasks, especially for 2D slices that contain a few pixels of ICH, but the high variability of CT slice thickness in the public datasets has posed challenges in the 3D approach. Recent developments in resolution-agnostic brain image segmentation (Billot et al., 2023) and image super-resolution (Sui et al., 2021) through generative DL models have allowed high-quality interpretation of clinical scans with diverse imaging protocols (e.g., different image resolutions). We will seek to adapt these frameworks for CT images in the task of ICH detection and segmentation in the future work.

7. Conclusion

To mitigate the requirement of expensive training data for intracranial hemorrhage segmentation, we have proposed a weakly supervised framework by using a novel hierarchical combination of head-wise gradient-infused self-attention maps from a Swin transformer through categorical learning. By using two public CT databases, we further demonstrated the benefits of head-wise gradient-weighting of derived attention maps to further boost ICH segmentation performance for the first time. In the future, we will further explore the proposed HGI-SAM technique and the application of the proposed weakly supervised segmentation framework in extended application and other Transformer models.

Acknowledgments

This work was supported by a Fonds de recherche du Quebec - Nature et technologies (FRQNT) Team Research Project Grant (2022-PR296459).

Ethical Standards

The work follows appropriate ethical standards in conducting research and writing the manuscript, following all applicable laws and regulations regarding treatment of animals or human subjects.

Conflicts of Interest

The authors declare no conflicts of interest for this work.

References

Trine Apostolaki-Hansson, Teresa Ullberg, Mats Pihlsgård, Bo Norrving, and Jesper Petersson. Prognosis of intracerebral hemorrhage related to antithrombotic use: an observational study from the swedish stroke register (riksstroke). *Stroke*, 52(3):966–974, 2021.

- Oren Barkan, Edan Hauon, Avi Caciularu, Ori Katz, Itzik Malkiel, Omri Armstrong, and Noam Koenigstein. Grad-sam: Explaining transformers via gradient self-attention maps. In *Proceedings of the 30th ACM International Conference on Information & Knowledge Management*, pages 2882–2887, 2021.
- Benjamin Billot, Douglas N. Greve, Oula Puonti, Axel Thielscher, Koen Van Leemput, Bruce Fischl, Adrian V. Dalca, and Juan Eugenio Iglesias. Synthseg: Segmentation of brain mri scans of any contrast and resolution without retraining. *Medical Image Analysis*, 86:102789, 2023. ISSN 1361-8415.
- Hila Chefer, Shir Gur, and Lior Wolf. Transformer interpretability beyond attention visualization. In *Proceedings of the IEEE/CVF Conference on Computer Vision and Pattern Recognition*, pages 782–791, 2021.
- Zhang Chen, Zhiqiang Tian, Jihua Zhu, Ce Li, and Shaoyi Du. C-cam: Causal cam for weakly supervised semantic segmentation on medical image. In *Proceedings of the IEEE/CVF Conference on Computer Vision and Pattern Recognition*, pages 11676–11685, 2022.
- Junghwan Cho, Ki-Su Park, Manohar Karki, Eunmi Lee, Seokhwan Ko, Jong Kun Kim, Dong-Eun Lee, Jaeyoung Choe, Jeongwoo Son, Myungsoo Kim, Sukhee Lee, Jeong-Eom Lee, Chang Hyo Yoon, and Sin youl Park. Improving sensitivity on identification and delineation of intracranial hemorrhage lesion using cascaded deep learning models. *Journal of Digital Imaging*, 32:450–461, 2018.
- Yin Dai, Yifan Gao, and Fayu Liu. Transmed: Transformers advance multi-modal medical image classification. *Diagnostics*, 11(8):1384, 2021. ISSN 2075-4418.
- Onat Dalmaz, Mahmut Yurt, and Tolga Çukur. Resvit: Residual vision transformers for multi-modal medical image synthesis. *IEEE Transactions on Medical Imaging*, pages 1–1, 2022.
- Alexey Dosovitskiy, Lucas Beyer, Alexander Kolesnikov, Dirk Weissenborn, Xiaohua Zhai, Thomas Unterthiner, Mostafa Dehghani, Matthias Minderer, Georg Heigold, Sylvain Gelly, Jakob Uszkoreit, and Neil Houlsby. An image is worth 16x16 words: Transformers for image recognition at scale. In *International Conference on Learning Representations*, 2021.
- Adam E Flanders, Luciano M Prevedello, George Shih, Safwan S Halabi, Jayashree Kalpathy-Cramer, Robyn Ball, John T Mongan, Anouk Stein, Felipe C Kitamura, Matthew P Lungren, et al. Construction of a machine learning dataset through collaboration: the rsna 2019 brain ct hemorrhage challenge. *Radiology: Artificial Intelligence*, 2(3), 2020.
- Wei Gao, Fang Wan, Xingjia Pan, Zhiliang Peng, Qi Tian, Zhenjun Han, Bolei Zhou, and Qixiang Ye. Ts-cam: Token semantic coupled attention map for weakly supervised object localization. In *Proceedings of the IEEE/CVF International Conference on Computer Vision*, pages 2886–2895, 2021.

- Yongqi Han, Lianglun Cheng, Guoheng Huang, Guo Zhong, Jiahua Li, Xiaochen Yuan, Hongrui Liu, Jiao Li, Jian Zhou, and Muyan Cai. Weakly supervised semantic segmentation of histological tissue via attention accumulation and pixel-level contrast learning. *Physics in Medicine and Biology*, 2022.
- Murtadha D Hssayeni, Muayad S Croock, Aymen D Salman, Hassan Falah Al-khafaji, Zakaria A Yahya, and Behnaz Ghoraani. Intracranial hemorrhage segmentation using a deep convolutional model. *Data*, 5(1):14, 2020.
- Hoel Kervadec, José Dolz, Shanshan Wang, Eric Granger, and Ismail Ben Ayed. Bounding boxes for weakly supervised segmentation: Global constraints get close to full supervision. *ArXiv*, abs/2004.06816, 2020.
- Kailu Li, Ziniu Qian, Yingnan Han, I Eric, Chao Chang, Bingzheng Wei, Maode Lai, Jing Liao, Yubo Fan, and Yan Xu. Weakly supervised histopathology image segmentation with self-attention. *Medical Image Analysis*, page 102791, 2023.
- Yu Liang, Maozhen Li, and Changjun Jiang. Generating self-attention activation maps for visual interpretations of convolutional neural networks. *Neurocomputing*, 490:206–216, 2022. ISSN 0925-2312.
- Huangjing Lin, Hao Chen, Qi Dou, Liansheng Wang, Jing Qin, and Pheng-Ann Heng. Scannet: A fast and dense scanning framework for metastatic breast cancer detection from whole-slide image. In *2018 IEEE winter conference on applications of computer vision (WACV)*, pages 539–546. IEEE, 2018.
- Geert Litjens, Robert Toth, Wendy Van De Ven, Caroline Hoeks, Sjoerd Kerkstra, Bram van Ginneken, Graham Vincent, Gwenael Guillard, Neil Birbeck, Jindang Zhang, et al. Evaluation of prostate segmentation algorithms for mri: the promise12 challenge. *Medical image analysis*, 18(2):359–373, 2014.
- Xiaoming Liu, Quan Yuan, Yaozong Gao, Kelei He, Shuo Wang, Xiao Tang, Jinshan Tang, and Dinggang Shen. Weakly supervised segmentation of covid19 infection with scribble annotation on ct images. *Pattern Recognition*, 122:108341, 2022. ISSN 0031-3203.
- Ze Liu, Yutong Lin, Yue Cao, Han Hu, Yixuan Wei, Zheng Zhang, Stephen Lin, and Baining Guo. Swin transformer: Hierarchical vision transformer using shifted windows. In *Proceedings of the IEEE/CVF International Conference on Computer Vision*, pages 10012–10022, 2021.
- John Muschelli. Recommendations for processing head ct data. *Frontiers in neuroinformatics*, 13:61, 2019.
- Jakub Nemcek, Tomas Vicar, and Roman Jakubicek. Weakly supervised deep learning-based intracranial hemorrhage localization. *arXiv preprint arXiv:2105.00781*, 2021.
- AI Qureshi and YY Palesch. Antihypertensive treatment of acute cerebral hemorrhage (atach) ii: design, methods, and rationale. *Neurocritical Care*, 15(3):559–576, 2011.

- Imran Qureshi, Junhua Yan, Qaisar Abbas, Kashif Shaheed, Awais Bin Riaz, Abdul Wahid, Muhammad Waseem Jan Khan, and Piotr Szczuko. Medical image segmentation using deep semantic-based methods: A review of techniques, applications and emerging trends. *Information Fusion*, 90:316–352, 2023. ISSN 1566-2535.
- Devika Rajashekar and John W Liang. Intracerebral hemorrhage. In *StatPearls [Internet]*. StatPearls Publishing, 2021.
- M. Rajchl, M. C. Lee, O. Oktay, K. Kamnitsas, J. Passerat-Palmbach, W. Bai, M. Damodaram, M. A. Rutherford, J. V. Hajnal, B. Kainz, and D. Rueckert. Deepcut: Object segmentation from bounding box annotations using convolutional neural networks. *IEEE Trans Med Imaging*, 36(2):674–683, 2017. ISSN 1558-254X (Electronic) 0278-0062 (Print) 0278-0062 (Linking).
- Amirhossein Rasoulia, Soorena Salari, and Yiming Xiao. Weakly supervised intracranial hemorrhage segmentation using hierarchical combination of attention maps from a swin transformer. In *Machine Learning in Clinical Neuroimaging: 5th International Workshop, MLCN 2022, Held in Conjunction with MICCAI 2022, Singapore, September 18, 2022, Proceedings*, pages 63–72. Springer, 2022. ISBN 978-3-031-17898-6.
- Holger R. Roth, Dong Yang, Ziyue Xu, Xiaosong Wang, and Daguang Xu. Going to extremes: Weakly supervised medical image segmentation. *Machine Learning and Knowledge Extraction*, 3(2):507–524, 2021.
- Hojjat Salehinejad, Jumpei Kitamura, Noah Ditzkofsky, Amy Lin, Aditya Bharatha, Suradech Suthiphosuwana, Hui-Ming Lin, Jefferson R Wilson, Muhammad Mamdani, and Errol Colak. A real-world demonstration of machine learning generalizability in the detection of intracranial hemorrhage on head computerized tomography. *Scientific Reports*, 11(17051), 2021.
- Ramprasaath R Selvaraju, Michael Cogswell, Abhishek Das, Ramakrishna Vedantam, Devi Parikh, and Dhruv Batra. Grad-cam: Visual explanations from deep networks via gradient-based localization. In *Proceedings of the IEEE International Conference on Computer Vision*, pages 618–626, 2017.
- Y. Sui, O. Afacan, A. Gholipour, and S. K. Warfield. Mri super-resolution through generative degradation learning. *Med Image Comput Comput Assist Interv*, 12906:430–440, 2021. doi: 10.1007/978-3-030-87231-1_42.
- Weixuan Sun, Jing Zhang, Zheyuan Liu, Yiran Zhong, and Nick Barnes. Getam: Gradient-weighted element-wise transformer attention map for weakly-supervised semantic segmentation. *arXiv preprint arXiv:2112.02841*, 2021.
- Kimberley M Timmins, Irene C van der Schaaf, Edwin Bennink, Ynte M Ruigrok, Xingle An, Michael Baumgartner, Pascal Bourdon, Riccardo De Feo, Tommaso Di Noto, Florian Dubost, et al. Comparing methods of detecting and segmenting unruptured intracranial aneurysms on tof-mras: The adam challenge. *Neuroimage*, 238:118216, 2021.

- Ostap Viniavskiy, Mariia Dobko, and Oles Doboisevych. Weakly-supervised segmentation for disease localization in chest x-ray images. In *Artificial Intelligence in Medicine: 18th International Conference on Artificial Intelligence in Medicine, AIME 2020, Minneapolis, MN, USA, August 25–28, 2020, Proceedings 18*, pages 249–259. Springer, 2020.
- Elena Voita, David Talbot, Fedor Moiseev, Rico Sennrich, and Ivan Titov. Analyzing multi-head self-attention: Specialized heads do the heavy lifting, the rest can be pruned. *arXiv preprint arXiv:1905.09418*, 2019.
- Risheng Wang, Tao Lei, Ruixia Cui, Bingtao Zhang, Hongying Meng, and Asoke K. Nandi. Medical image segmentation using deep learning: A survey. *IET Image Processing*, 16(5):1243–1267, 2022.
- Ross Wightman. Pytorch image models. <https://github.com/rwightman/pytorch-image-models>, 2019.
- Kai Wu, Bowen Du, Man Luo, Hongkai Wen, Yiran Shen, and Jianfeng Feng. Weakly supervised brain lesion segmentation via attentional representation learning. In *Medical Image Computing and Computer Assisted Intervention - MICCAI 2019*, pages 211–219. Cham, 2019. Springer International Publishing.
- Hai Ye, Feng Gao, Youbing Yin, Danfeng Guo, Pengfei Zhao, Yi Lu, Xin Wang, Junjie Bai, Kunlin Cao, Qi Song, Heye Zhang, Wei Chen, Xuejun Guo, and Jun Xia. Precise diagnosis of intracranial hemorrhage and subtypes using a three-dimensional joint convolutional and recurrent neural network. *European Radiology*, 29:6191–6201, 2019.
- Daquan Zhou, Bingyi Kang, Xiaojie Jin, Linjie Yang, Xiaochen Lian, Qibin Hou, and Jiashi Feng. Deepvit: Towards deeper vision transformer. *ArXiv*, abs/2103.11886, 2021.
- Zhi-Hua Zhou. A brief introduction to weakly supervised learning. *National Science Review*, 5(1):44–53, 2017.